Plasma Immersion Ion Implantation for SOI Synthesis: SIMOX and Ion-Cut

XIANG LU,[1] S. SUNDAR KUMAR IYER,[1] JIN LEE,[2] BRIAN DOYLE,[2] ZHINENG FAN,[3] PAUL K. CHU,[3] CHENMING HU,[1] and NATHAN W. CHEUNG[1]

1.— Electronics Research Laboratory, University of California at Berkeley, CA 94720-1770. 2.— Components Research, Intel Corporation, Santa Clara, CA 95052. 3.— Department of Physics and Materials Science, City University of Hong Kong, Kowloon, Hong Kong

We have demonstrated feasibility to form silicon-on-insulator (SOI) substrates using plasma immersion ion implantation (PIII) for both separation by implantation of oxygen and ion-cut. This high throughput technique can substantially lower the high cost of SOI substrates due to the simpler implanter design as well as ease of maintenance. For separation by plasma implantation of oxygen wafers, secondary ion mass spectrometry analysis and cross-sectional transmission electron micrographs show continuous buried oxide formation under a single-crystal silicon overlayer with sharp Si/SiO_2 interfaces after oxygen plasma implantation and high-temperature (1300°C) annealing. Ion-cut SOI wafer fabrication technique is implemented for the first time using PIII. The hydrogen plasma can be optimized so that only one ion species is dominant in concentration and there are minimal effects by other residual ions on the ion-cut process. The physical mechanism of hydrogen induced silicon surface layer cleavage has been investigated. An ideal gas law model of the microcavity internal pressure combined with a two-dimensional finite element fracture mechanics model is used to approximate the fracture driving force which is sufficient to overcome the silicon fracture resistance.

Keywords: Fracture mechanics, hydrogen plasma, plasma immersion ion implantation (PIII), separation by implantation of oxygen (SIMOX), silicon on insulator (SOI)

INTRODUCTION

Plasma immersion ion implantation (PIII) is an emerging technology for high dose-rate implantation.[1-3] The physical principle of PIII is illustrated in Fig. 1. A substrate is placed on a holder which is immersed into a uniform plasma containing the implant ion species. A negative bias voltage, which can be DC or transient pulse, is applied to the substrate holder. When this bias voltage is applied, electrons are repelled away from the target surface and a sheath is established. The positive ions will be accelerated by the negative substrate bias and eventually implanted. Since no mass separation is utilized in the PIII method, composition of the ion species is mainly controlled by the gas composition and plasma excitation.

The major advantage of PIII over conventional implanter is its high throughput for high dose processing (e.g. silicon-on-insulator or SOI) and large area processing (e.g. flat panel display). Since the entire wafer is implanted simultaneously in PIII, the processing time is independent of the wafer size. This contrasts sharply with conventional implantation where an ion beam is scanned across the wafer and the implantation time scales with the square of the wafer radius. An implantation throughput comparison between PIII and a state-of-the-art high current conventional implanter is illustrated in Fig. 2, using a dose requirement of 10^{18} cm^{-2}. In this comparison, we use the current density for PIII because the implantation is independent of area. It should also be mentioned that conventional ion implantation is a batch process whereas PIII is not. However, in using a multiple sample exchange mechanism, the sample exchange time is minimal compared to the actual implantation time. The time saving, especially for larger wafers, is thus quite substantial. PIII also offers simple machine design and maintenance, full compatibility with integrated-circuit processing clus-

(Received June 20, 1997; accepted May 29, 1998)

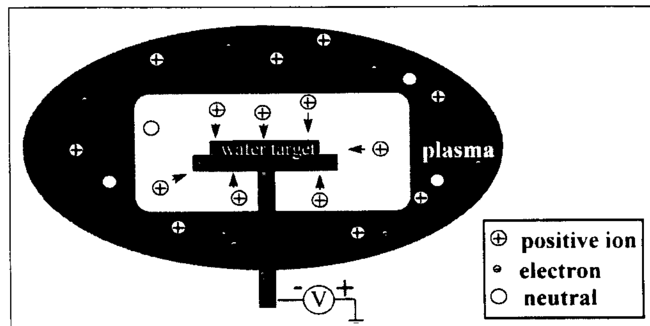

Fig. 1. Schematic illustration of physical principle of plasma immersion ion implantation (PIII).

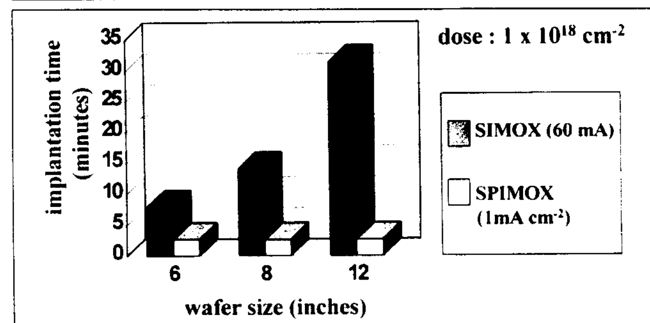

Fig. 2. Throughput comparison between conventional SIMOX process and SPIMOX process. Since the whole wafer is implanted simultaneously, the rate of the SPIMOX implantation is independent of the wafer size.

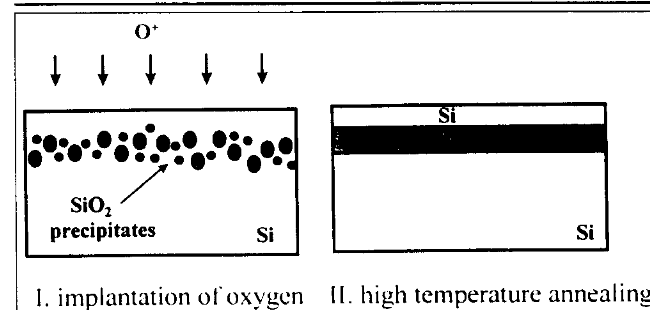

Fig. 3. Schematic of the SIMOX process, which includes two major processing steps: implantation of oxygen and high temperature annealing.

ter tools, and conformal implantation capability.

The semiconductor applications currently under development using PIII systems are shallow junction formation in integrated circuits,[4,5] SIMOX and ion-cut SOI wafer fabrication,[6–10] doping and hydrogenation for flat-panel display thin-film transistors,[11,12] and trench sidewall doping.[13] In this paper, we report mainly application of PIII for SIMOX and ion-cut SOI wafer fabrication.

Among SOI technologies, SIMOX is considered to be the most mature and promising for high density CMOS circuits. There are two major wafer fabrication steps in the SIMOX process: implantation of oxygen and high temperature annealing, as shown in Fig. 3. Both processing steps are similar to those used in conventional integrated circuit fabrication process, but the requirements are quite different. The oxygen implantation dose is quite high, and wafer temperature needs to be maintained at certain temperature,

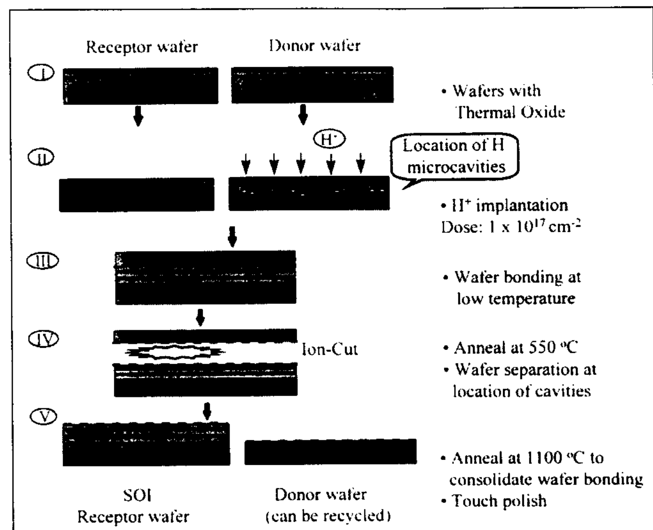

Fig. 4. Process flow of ion-cut SOI fabrication. Note the donor wafer after cleavage can be recycled as receptor wafer.

typically around 650°C. The post annealing temperature is above 1300°C and much higher than a typical IC process.

SIMOX SOI wafers are costly to manufacture due to the long implantation time required for the high oxygen dose (2×10^{17}–2×10^{18} cm^{-2}). Attempts have been made to develop high current implanters specific to SIMOX applications.[14,15] Low dose, thin SIMOX processes that require shorter implantation time have also been considered,[16–18] which result in shorter implantation time. Our recent work on separation by plasma implantation of oxygen (SPIMOX), which is a modification of the conventional SIMOX process, uses the plasma immersion ion implantation process.[6–9] This process allows for even higher throughput for implanting SIMOX wafers.

Recently, there is an emerging technology, ion-cut, commercially referred as Smart-Cut™[19,20] that has advantages of both the SIMOX and BESOI (wafer bonding and etch back SOI) features. The implantation step of the ion-cut process provides the excellent uniformity of the top silicon thickness. The thermal growth of oxide and wafer bonding provide high quality and uniformity of the buried oxide with an arbitrary thickness. Furthermore, ion-cut opens up other exciting material synthesis opportunities for the electronics industry, such as silicon-on-glass,[21] germanium, silicon-carbide, diamond thin films,[22] and even three-dimensional stacking of devices.[23,24]

The ion-cut process has been described in the literature.[19,20] The process flow is illustrated in Fig. 4. This process starts with a donor wafer and a receptor wafer, with one or both wafers grown with thermal oxide. Hydrogen is implanted into the donor wafer coated with thermal oxide. The donor wafer is then bonded with the receptor silicon wafer. The wafer bonding and curing temperature is typically less than 300°C. The bonded wafer pair is then subjected to a cleavage thermal treatment between 400 to 600°C. During the cleavage thermal treatment, the wafer

pair breaks into two completely separated wafers along the hydrogen implanted depth, and the receptor wafer has now an SOI structure. A high temperature annealing process (i.e., 1100°C) is then performed to perfect the wafer bonding interface. The wafer surface is finally touch polished to make an integrated-circuit grade SOI wafer. Because the donor wafer can be touch polished and then recycled as the receptor wafer, this process will not waste substrate materials.

In the ion-cut process, the required hydrogen dose is also quite high and in the range of 2×10^{16} to 1×10^{17} atoms-cm^{-2}. PIII is well-suited for this high dose application. PIII may also provide other ion-cut process optimization opportunities, such as multiple ion implantation, and surface plasma treatment for low temperature wafer bonding.

OPTIMIZATION OF PLASMA CONDITIONS FOR PIII

Our PIII system setup is illustrated in Fig. 5. The target wafer is immersed in the oxygen or hydrogen plasma and a negative DC bias is applied to it. At a sufficiently low chamber pressure (less than 200 μTorr), the mean free path of the ions is much larger than the sheath thickness, and ion transport across the sheath can be assumed collisionless. Under these conditons, the implantation energy is equal to the applied bias voltage.

The plasma is generated using an electron cyclotron resonance (ECR) source with a microwave frequency of 2.45 GHz. The magnetic field for the ECR plasma is generated using a DC current source through copper coils. The plasma ion densities were monitored using a SXP 300 VG quadrupole in connection with a CMX 500 cylindrical mirror energy analyzer. The plasma conditions have been tuned by mainly varying the oxygen or hydrogen gas pressure, microwave power, and magnetic coil current.

As the implantation system does not use mass selection, both O^+ and O_2^+ generated by the ECR oxygen plasma will be implanted in the SPIMOX process. However, to generate a single nucleation plane for the SPIMOX, we have to ensure that one ion species dominates the implant and a single peaked implant profile is formed in the wafer. We have chosen O_2^+ as the dominant ion species in the plasma. Mass spectrometer measurements of the plasma ions showed that over 92 percent of the ions are O_2^+, while less that 8 percent is O^+ (Fig. 6). Since every O_2^+ ion carries 2 oxygen atoms, the oxygen dose due to O_2^+ implant is over 95 percent, while the dose due to O^+ is less than 5 percent. The effect of O^+ implantation on oxide nucleation is undetectable after the high temperature annealing.

For the hydrogen PIII ion-cut process, the simultaneous presence of H^+, H_2^+, and H_3^+ in the plasma is a consideration. For example, the presence of multiple peaks in the hydrogen depth profile may initiate cleavage at different depths. It is found that hydrogen gas pressure has the most significant effect on the ion composition. As shown in Fig. 7, H^+ ions constitute about 20% for all gas pressure investigated. On the other hand, H_3^+ ions are found to increase dramatically from less than 3% at 75 μTorr to 75% at 1 mTorr. H_2^+ ions are found to decrease from 80 to 5% in the same pressure range. The magnetic coil current is at I = 220 A and the input microwave power is at P = 300 W for all the hydrogen pressure conditions. Both the

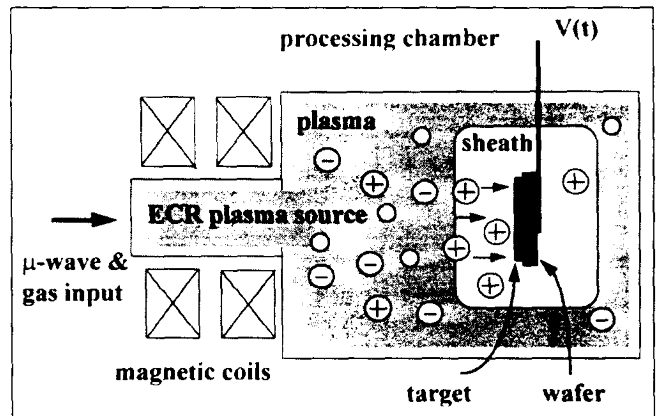

Fig. 5. Schematic of the Berkeley PIII system. The target wafer is immersed in a quasi-neutral plasma and a negative DC bias corresponding to the desired implantation energy is applied to the target. A typical implantation dose rate is around $10^{15} \sim 10^{16}$ cm^{-2}s^{-1}.

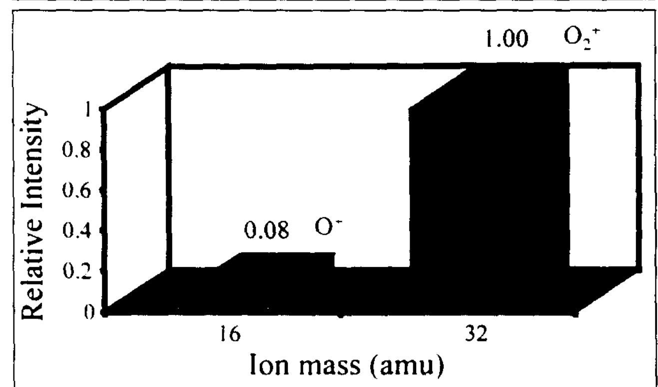

Fig. 6. Oxygen plasma ion composition measured by mass spectrometry. The oxygen gas pressure is 75 μTorr and a microwave power of 300 W was used.

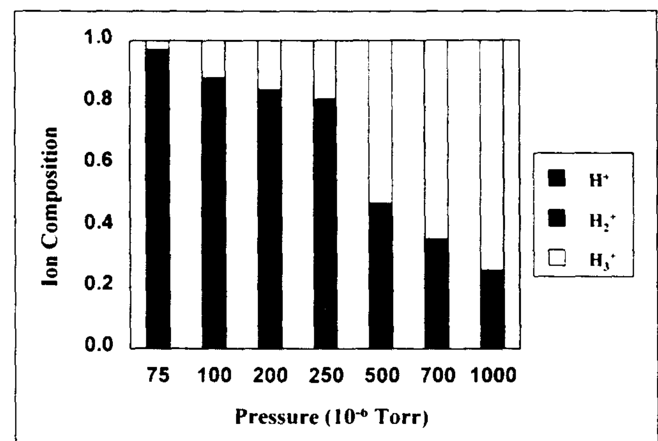

Fig. 7. Hydrogen plasma ion composition at different chamber pressure, measured by mass spectrometry. The microwave power is 300 W.

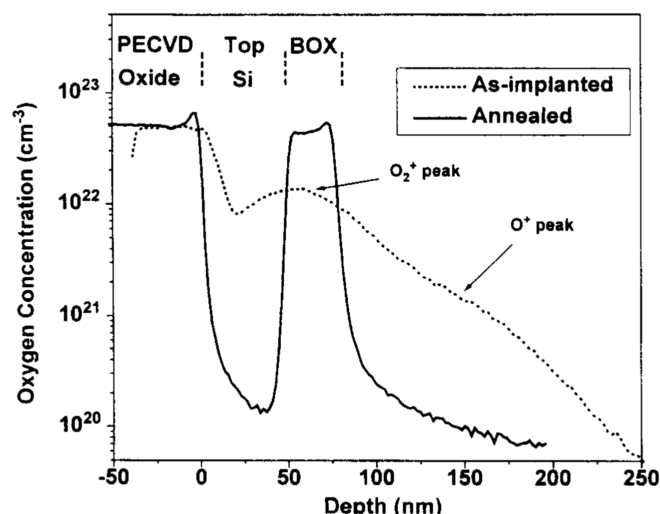

Fig. 8. SIMS profile of the oxygen concentration of as-implanted and annealed silicon wafer using SPIMOX. The implantation was carried out at 60 kV. The wafer was annealed at 1300° for 3h.

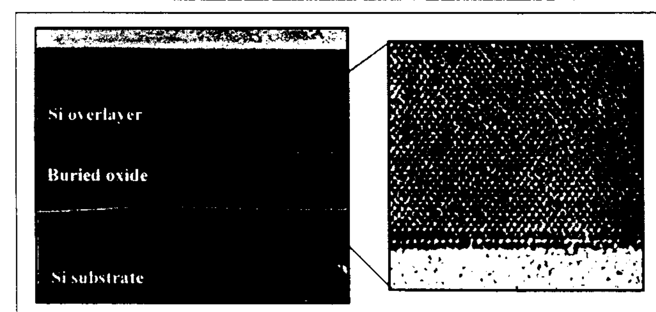

Fig. 9. XTEM micrograph of the SOI structure formed using the SPIMOX process. The implantation was carried out at 60 kV. The wafer was annealed at 1300°C for 3 h. Single crystal silicon over-layer is formed with abrupt Si/oxide interfaces.

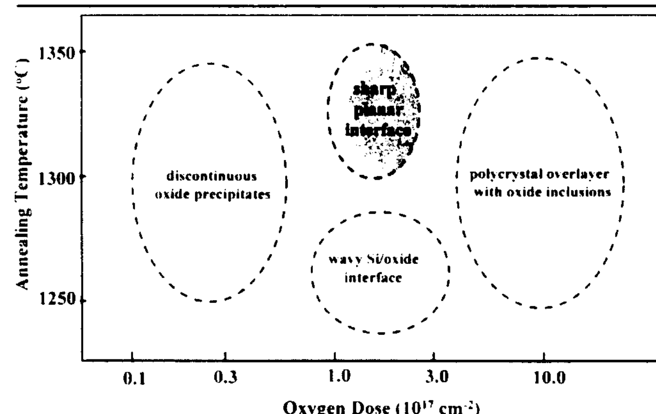

Fig. 10. SPIMOX process window in terms of the oxygen dose and the annealing temperature. The optimal dose for −60 kV implantation is at 1–2 × 10^{17} cm^{-2}, and the optimal annealing temperature is over 1300°C.

magnetic coil current and microwave power have shown lesser effects on the ion composition.

We have chosen H_2^+ as the dominant implantation species for the PIII ion-cut process for the following two reasons. Firstly, H_2^+ is dominant at the lower pressure regime, while the total ion density is also lower. Therefore, the implantation current is lower with H_2^+ as the dominant ion species and less heating results during implantation. By keeping the wafer temperature during implantation below 250°C, the implanted hydrogen is less likely to diffuse and nucleate during the implantation step. Secondly, H_2^+ can offer a larger implantation penetration depth comparing with H_3^+.

SPIMOX WAFER FABRICATION RESULTS

SPIMOX Experimental

CZ grown, 4 inch p-type <100> silicon wafers were used to fabricate SOI structures using the SPIMOX process. The oxygen gas pressure in the implantation chamber was kept between 50 and 100 μTorr. The coupled microwave power was at between 200 and 300 W. The wafer was biased at −60 kV. Rough temperature measurements using pyrometer showed that the substrate temperature was about 600 to 700° during PIII.

After implantation, wafers were capped with 300 nm oxide and 200 nm nitride passivation layers using plasma enhanced chemical vapor deposition (PECVD). The nitride capping layers are necessary to prevent the oxidation of the thin silicon over-layer during the high temperature furnace annealing, while the oxide layer makes the silicon surface layer stress free. A typical post-implantation annealing consisted of three stages: 800°C for 1 h; 1000°C for 1 h; and 1300 to 1325°C for 3 h, all in a nitrogen ambient. The temperature ramp rate was approximately 5 degrees per minute.

SIMS Oxygen Profile

The oxygen profiles of the as-implanted and annealed wafers acquired by SIMS are displayed in Fig. 8. The implantation voltage is 60 kV with an oxygen dose of 1 × 10^{17} cm^{-2}. As expected, there is only one dominant oxygen peak, corresponding to the implanted O_2^+. After annealed at 1300°C for 3 h, a complete BOX layer is formed. The stoichiometry of the BOX layer is identical to the passivation PECVD oxide layer deposited at the wafer surface, indicated by the same level of oxygen signal in both the buried oxide layer and the surface PECVD layer. The SIMS data of the annealed wafer also show a very sharp silicon/oxide interface.

XTEM Characterization

Cross-sectional transmission electron microscopy (XTEM) was performed using a JEOL JEM 200CX microscope operating at 200 kV to examine the SOI structure morphology. A cross-sectional TEM picture of an annealed SPIMOX sample is shown in Fig. 9. A continuous, planar buried oxide layer is formed under a single crystal silicon over-layer. The abrupt silicon/oxide interface is shown in the insert of a high-resolution TEM micrograph. In the SPIMOX wafer shown, the buried oxide thickness is 25 nm while the top silicon thickness is 50 nm.

SPIMOX Operational Phase Space

If the oxygen dose is too low (less than 5 × 10^{16}

cm^{-2}), discontinuous oxide precipitates will form instead of a continuous buried oxide layer. On the other hand, excessive oxygen dose (more than 3×10^{17} cm^{-2}) leaves a high oxygen concentration in the over-layer silicon, and forms oxide inclusions in the over-layer. If the final annealing temperature is not high enough (less than 1275°C), the silicon/oxide interfaces undulate, and the BOX layer thickness varies microscopically across the wafer. The process phase space in terms of the oxygen dose and the annealing temperature is summarized in Fig. 10. It shows the SPIMOX process window in terms of the oxygen dose and the annealing temperature using –60 kV bias. A continuous BOX structure requires an oxygen dose between 1×10^{17} cm^{-2} to 3×10^{17} cm^{-2} and a planar oxide interface requires annealing temperature above 1300°C.

ION-CUT PHYSICAL MECHANISMS

The present understanding of the ion-cut process is illustrated in Fig. 11. After the hydrogen implantation, the trapped hydrogen atoms combine with silicon atoms forming a Si-H complex. This Si-H bond formation was first detected using infrared spectroscopy measurement by Weldon et al.[25,26] During thermal annealing, the trapped hydrogen atoms diffuse and segregate near the peak implantation region, forming microcavities filled with H_2 molecules.[27] Under further annealing, it is proposed that more hydrogen diffuses into the microcavities, where a high pressure inside the microcavity becomes the driving force for its expansion and growth. In case (a), if a surface stiffener such as a bonded wafer is capped on the implanted wafer surface, these microcavities grow along the (001) plane during annealing, parallel to the wafer surface. When these microcavities grow larger, more hydrogen atoms diffuse in, keeping the internal pressure high for continuous expansion. Meanwhile, the microcavities will coalesce forming even larger cavities. When all the cavities are linked together, the bonded wafer pair becomes completely separated along the cavity plane. In case (b), if no capping layer is present on the implanted wafer surface, a similar mechanism will cause the microcavities to nucleate and grow under thermal annealing. However, the microcavity expansion and growth can easily derail and penetrate through the surface layer due to the absence of the stiffener, causing blistering of the surface silicon layer, as shown in Fig. 11.

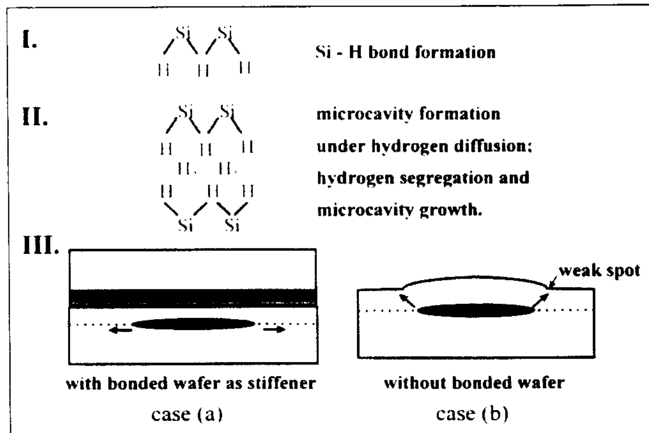

Fig. 11. Proposed physical mechanisms of ion-cut process. For case (a) the bonded wafer acts as a stiffener to confine the fracture propagation along the plane of the implanted hydrogen depth.

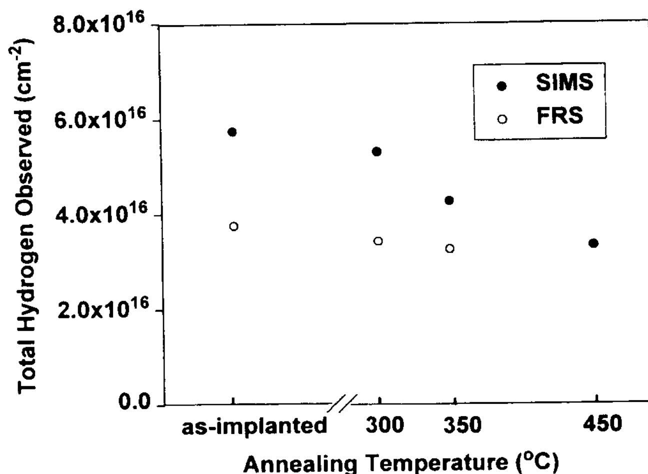

Fig. 12. Hydrogen concentration from SIMS and FRS measurements. A nominal hydrogen dose of 4×10^{16} cm^{-2} was implanted at 40 kV using a conventional implanter with H^+ ions.

Hydrogen Concentration Measurements

To investigate the hydrogen induced cleavage mechanism, we have performed a controlled experiment using conventional ion implantation of H^+ ions at 40 kV into silicon substrates. Hydrogen profiles are measured by both SIMS and hydrogen forward scattering (HFS) experiments. The hydrogen dose from both SIMS and HFS are plotted in Fig. 12. There is some discrepancy on the absolute value of the hydrogen dose due to systematic errors in the SIMS data. The dose value from the SIMS data is generally less accurate (±20% error) due to its indirect calibration method. On the other hand, HFS experiments have less error in the absolute value, and the HFS measurement results agree well with the dose value calibrated by hydrogen implantation current (4×10^{16} cm^{-2}). Nevertheless, the same dose variation trend is found from both techniques. The hydrogen profile and total dose are largely preserved after annealing up to 350°C, just before the cleavage layers break through the surface. Although the hydrogen diffusion constant in silicon is known to be high (~2.8×10^{-9} cm^2/s at 400°C),[28] our observed large hydrogen retention suggests the dominant gettering role of microcavity nucleation.

Microcavity Internal Pressure

Based on the total hydrogen dose measurement results, the internal stresses caused by the molecular hydrogen is estimated using the ideal gas law. We assume a hydrogen implantation dose of 5×10^{16} cm^{-2}, and half of the hydrogen is nucleated inside the microcavities after certain annealing. We further assume the microcavities have a uniform thickness of

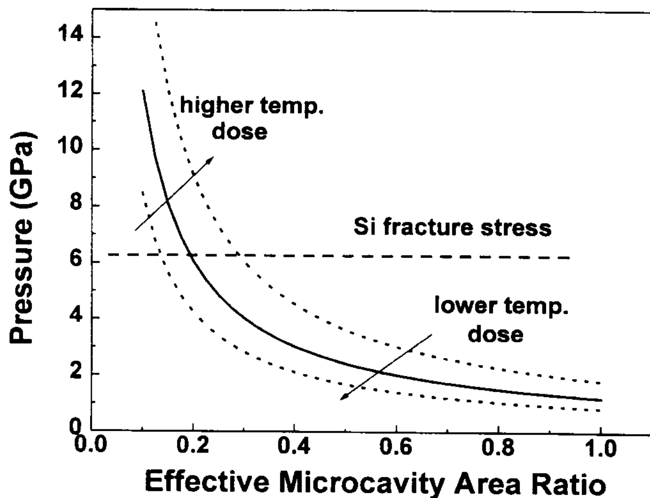

Fig. 13. Microcavity internal pressure vs the effective area ratio. The retained hydrogen dose is taken to be 5×10^{16} cm^{-2}, and the annealing temperature is at 300°C. The calculated internal pressure is based on the ideal gas law.

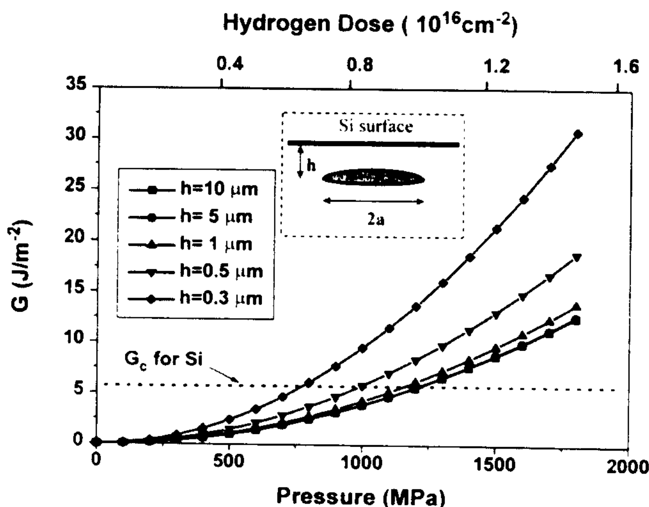

Fig. 14. Finite element method modeling of fracture driving force at different microcavity depths. The crack radius used in the calculation is 0.5 μm. Note virtually the same fracture driving force results are obtained when the crack is located deep from the surface (i.e., h = 5 μm and h = 10 μm).

1 nm, a value observed by cross-sectional TEM. The H_2 molecule density in the cavities is 1.3×10^{23} cm^{-3}. Using the ideal gas law, the calculated internal pressure values inside the microcavities at 300°C are determined. The pressure values are plotted as a function of the effective microcavity area ratio, defined by the projected areas covered with microcavities normalized by the whole wafer area. As shown in Fig. 13, the hydrogen gas pressures are in the Giga-Pascal (GPa) range. Previously reported fracture stress value for single crystal silicon is 6.1 GPa using a microbeam setup experiment.[29] We expect that the fracture stress in the hydrogen peak regions could be less than the perfect silicon crystal value, considering the fact that hydrogen super-saturation and the implantation damage can generate many dangling bonds in silicon. Even though in reality, the hydrogen microcavities are scattered about the peak and not concentrated within a thickness of 1 nm,[30] this simple order-of-magnitude calculation supports the argument that the internal pressure inside the microcavities is strong enough to break the Si-Si bond, thus causing the surface layer cleavage.

Finite Element Fracture Mechanics Modeling

It is believed that crack propagation occurs when the energy available for crack growth is sufficient to overcome the fracture resistance of the material.[31,32] This can be stated as an energy balance criterion between the energy release rate (G), which is defined as the rate of change in potential energy with crack area for a linear elastic material and the fracture toughness (G_c), which include the surface energy, plastic work, or other types of energy dissipation associated with a propagating crack. The energy release rate (G) is also called the fracture driving force. Therefore, one needs to know G and G_c to determine if a given crack will grow or not. G varies with geometry including crack size (radius a), depth location (h) and the applied loading. G_c is a material parameter and, it is around 6.2 J/m^2 for silicon.[33]

The initial microcavity in silicon substrate induced by the hydrogen segregation is modeled as a circular crack which is embedded at a certain depth (h) from the top silicon surface. The ABAQUS program[34] based on two-dimensional finite element analysis was used to calculate the energy release rate (G) under the applied internal pressure (P) along the crack surfaces. In this simulation, silicon is treated as a linear elastic and isotropic material. Young's modulus and Poisson's ratio for silicon are taken as 149.6 GPa and 0.28, respectively.[31] The numerical error of the finite element model is less than 0.3% when compared with analytical solutions for the special case where the microcavity is buried very deep into the substrate (i. e., h = 10 μm and a = 0.5 μm).

Figure 14 shows the energy release rate (G) for a crack of size 0.5 μm (a = 0.5 μm) at different depths. The critical pressure (P_{cr}) to meet the energy balance criterion for the crack to propagate increases with depth (h); P_{cr} is 800 MPA for h = 0.3 μm, 1 GPA for h = 0.5 μm, and 1.2 GPa for h = 1 μm or larger. The energy release rate (G) is proportional to the square of internal pressure (P) as predicted by analytical model.[31,32] An equivalent hydrogen dose axis is given in Fig. 14 based on the ideal gas law assumption, with an annealing temperature of 30°C and an effective microcavity area ratio of 0.5.

ION-CUT WAFER FABRICATION RESULTS

CZ-grown (100), p-type, 5–10 ohm-cm, 4 inch silicon wafers with 120 nm thermal oxide were used in this PIII study. A negative bias of 30 to 60 kV was applied to the wafer. The nominal hydrogen atomic dose was between 1×10^{16} to 2×10^{17} cm^{-2}. The implantation time was less than 2 min even for the highest dose. The silicon wafers were maintained at below 200°C during the plasma implantation. The

implanted donor wafer is then RCA-cleaned and hydrophilically bonded with the receptor wafer at room temperature. The bonded wafer pair was annealed in a nitrogen ambient at 200°C to enhance the bonding strength. Then the wafer pair was elevated to higher annealing temperatures between 500 and 650°C to accomplish the wafer cleavage. Finally, the SOI structure was annealed between 900 to 1100°C for 60 min in nitrogen ambient to enhance the oxide interface bonding.

SIMS Profile of PIII Hydrogen

A plasma condition is used at which there were over 90% H_2^+ ions, less than 10% H^+ and negligible H_3^+ ions. These conditions were achieved at a chamber pressure between 75 and 100 µTorr, a magnetic coil between 180 to 190 A, and 300 W microwave power. SIMS profile of a 50 kV implanted sample using such hydrogen plasma conditions is plotted in Fig. 15. As shown, over 95% of the hydrogen dose is from H_2^+ while less than 5% is from H^+. Implant concentration from H_3^+ ions is not detectable. According to TRIM92 simulation, the projected ranges for 50 kV H_2^+ and H^+ implantation are at 296 nm µm and 493 nm, respectively, in good agreement with ther SIMS profiles.

PIII Hydrogen Ion-Cut SOI Structure

A $Si/SiO_2/Si$ structure fabricated using the hydrogen PIII ion-cut process is shown in Fig. 16. The top silicon wafer was implanted using the H_2^+ dominated plasma at 35 kV and a nominal hydrogen atomic dose of 1×10^{17} cm^{-2}. The wafer separation is uniform across the sample surface, and there is no silicon layer separation along the H^+ or H_3^+ implanted depths. The dashed line indicates the original bonded oxide/oxide interface. Apparently after the 900°C 60 min final annealing, there is no distinguishable interface in the bonded oxide layer.

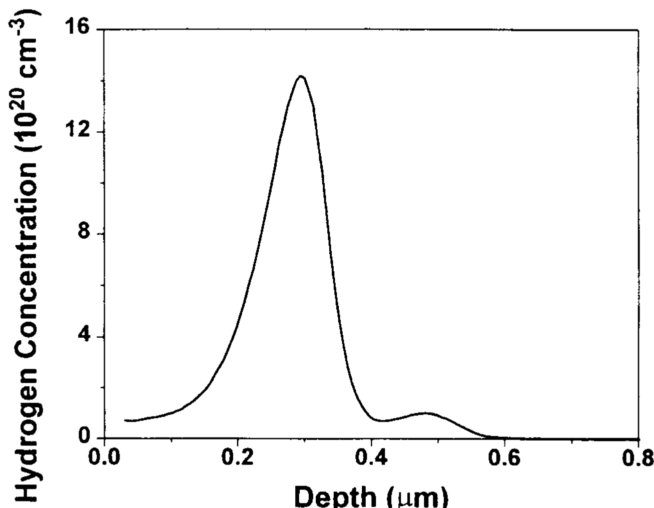

Fig. 15. SIMS profile of PIII hydrogen. More than 95% of hydrogen dose is from H_2^+ implantation, while less than 5% dose is from H^+. The implantation voltage is 50 kV with a nominal dose of 1×10^{15} cm^{-2}.

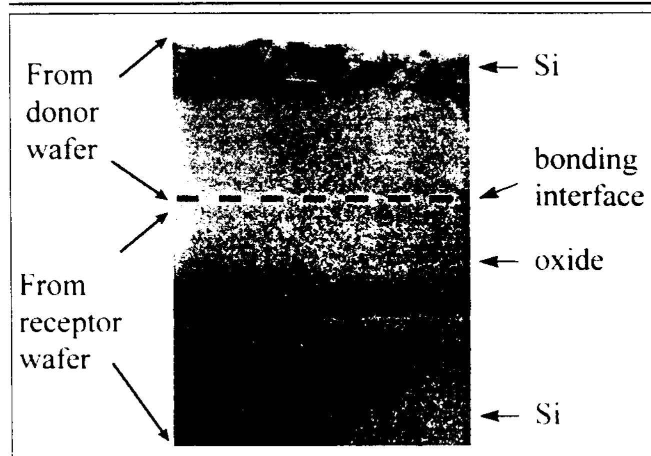

Fig. 16. XTEM micrograph of SOI structure formed using hydrogen PIII ion-cut process. The donor wafer was implanted using hydrogen plasma at 35 kV with 10^{17} cm^{-2} nominal dose.

SUMMARY

We have employed PIII of oxygen to synthesize SIMOX structure and PIII of hydrogen to perform the ion-cut process. The feasibility of SPIMOX has been demonstrated with successful fabrication of SOI structures. The operational phase space on oxygen dose and annealing temperature has been identified. The ion-cut SOI wafer fabrication technique is also implemented using PIII. The simple PIII reactor setup and its compatibility with cluster-tool IC manufacturing equipment offer other ion-cut process optimization opportunities. The hydrogen plasma can be optimized so that only one ion species is dominant in concentration, with minimal effect on the ion-cut process by the residual ion components. We have also investigated the physical mechanisms of hydrogen induced silicon surface layer cleavage. Estimation using an ideal gas law model calculation suggests that internal pressure of molecular hydrogen filled microcavities is in the range of Giga-Pascal and high enough to break silicon crystal bonds. ABAQUS two-dimensional finite element method (FEM) model of the structure predicts that the energy release rate (G) is sufficient to overcome the silicon fracture resistance (G_c).

ACKNOWLEDGMENTS

The authors would like to thank J. Min, J. Liu, Q.Y. Tong, T.H. Lee and M. Strathman for their contributions to the work described in this paper. The XTEM experiments were performed at the National Center for Electron Microscopy (NCEM) at Lawrence Berkeley National Laboratory (LBNL). This work is sponsored by Joint Services of Electronics Program under Contract F49620-94-C-0038, National Science Foundation under Contract 442427, and Hong Kong RGC Earmarked Grants 9040220 and 9040332.

REFERENCES

1. N.W. Cheung, W. En, J. Gao, S.S.K. Iyer, E.C. Jones, B.P. Linder, J.B. Liu, X. Lu, J. Min and B. Shieh, *1995 Intl. Conf. on Solid State Dev. and Mat. Ext. Abs.*, (Osaka, Japan, 1995), p. 351.
2. E.C. Jones, B.P. Linder and N.W. Cheung, *Jpn. J. Appl. Phys.* 35, Part 1, (2B), 1027 (1996).

3. P.K. Chu, S. Qin, C. Chan, N.W. Cheung and L.A. Larson, *Mater. Sci. and Eng.* R17 (6–7), 207 (1996).
4. E.C. Jones, S. Im and N.W. Cheung, *Beam-Solid Interactions: Fundamentals and Applications,* 279, ed. M. Nastasi, (Pittsburgh, PA: Mater. Research Society, 1993), p. 255.
5. E.C. Jones and N.W. Cheung, *IEEE Elec. Dev. Lett.* 14 (9), 444, (1993).
6. L. Zhang, J.L. Shohet, D. Dallmann, J.H. Booske, R.R. Speth, K. Shenai, M.J. Goeckner, J.B. Kruger, P. Rissman, J.E. Turner, E. Perez-Albuerne, S. Lee and N. Meyyappan, *Appl. Phys. Lett.* 65 (8), 962 (1994).
7. J.B. Liu, S.S.K. Iyer, C. Hu, N.W. Cheung, R. Gronsky, J. Min and P.Chu, *Appl. Phys. Lett.* 67 (16), 2361 (1995).
8. X. Lu, S.S.K. Iyer, J.B. Liu, J. Min, P.K. Chu, C. Hu and N.W. Cheung, *Appl. Phys. Lett.* 70 (13),1750 (1997).
9. X. Lu, S.S.K. Iyer, J. Min, Z. Fan, J.B. Liu, P.K. Chu, C. Hu and N.W. Cheung, *1996 IEEE Intl. SOI Conf. Proc.* 48–49, (1996).
10. X. Lu, Ph. D dissertation, University of California, Berkeley, (1997).
11. J.D. Bernstein, S. Qin, C. Chan and T. J. King, *IEEE Tran. Elect. Dev.* 43 (11) 1876 (1996).
12. J.D. Bernstein, S. Qin, C. Chan and T.-J. King, *IEEE Elect. Dev. Lett.* 16 (10), 421 (1995).
13. C. Yu and N.W. Cheung, *IEEE Electron Dev. Lett.* 15 (6), 196 (1994).
14. G. Ryding, T.H. Smick, M. Farley, B.F. Cordts, R.P. Dolan, L.P. Allen, B. Mathews, W. Wray, B. Amundsen and M.J. Anc, *Proc. Eleventh Intl. Conf. on Ion Implantation Technology*, Austin, Texas, (1996), p. 436.
15. K. Tokiguchi, T. Seki, K. Amemiya and Y. Yamashita, *Proc. Eleventh Intl. Conf. on Ion Implantation Technology*, Austin, Texas, (1996), p. 287.
16. A.K. Robinson, C.D. Marsh, U. Bussmann, J.A. Kilner, Y. Li, J. Vanhellemont, K.J. Reeson, P.L.F. Hemment and G.R. Booker, *Nuclear Instruments and Methods B* 55, 555 (1991).
17. F. Namavar, E. Cortesi, N.M. Kalkhoran and J.M. Manke, *Proc. IEEE SOS/SOI Technology Workshop*, (New York: IEEE, 1990), p. 49.
18. M. Alles, W. Krull and L. Allen, *Proc. Sixth Intl. Symp. on Silicon-On-Insulator Technology and Devices* (1994), p. 459.
19. M. Bruel, B. Aspar, B. Charlet, C. Maleville, T. Poumeyrol, A. Soubie, A J. Auberton-Herve, J.M. Lamure, T. Barge, F. Metral and S. Trucchi, *1995 IEEE Intl. SOI Conf. Proc.*, Tucson, Arizona, (New York: IEEE, 1995), p. 178.
20. M. Bruel, *Nuclear Instruments and Method in Physical Research,* B108, 313 (1996).
21. Q.Y. Tong, T.H. Lee, W.J. Kim, T.Y. Tan, U. Gosele, H.M. You, W. Yun and J.K.O. Sin, *1996 IEEE Intl. SOI Conf. Proc.*, Sanibel Island, Florida, (1996), p. 36.
22. Q.Y. Tong, T.H. Lee, K. Gutjahr, S. Hopfe and U. Gosele, *Appl. Phys. Lett.* 1390 (1996).
23. B.H. Lee, G.J. Bae, K.W. Lee, G. Cha, W.D. Kim, S.I. Lee, T. Barge, A. J. Auberton-Herve and J.M. Lamure, *1996 IEEE Intl. SOI Conf. Proc.,* 114, Sanibel Island, Florida, (1996), p. 114.
24. B. Aspar, M. Bruel, M. Zussy and A.M. Cartier, *Electron. Lett.* 32 (21), 1985 (1996).
25. M.K. Weldon, V. Marsico, Y.J. Chabal, S.B. Christman, E.E. Chaban, D.C. Jacobson, J.B. Sapjeta, A. Pinczuk, B.S. Dennis, A.P. Mills, C.A. Goodwin and C.M. Hsieh, *1996 IEEE Intl. SOI Conf. Proc.* Sanibel Island, Florida, (1996), p. 150.
26. M.K. Weldon, V. Marsico, Y.J. Chabal, A. Agarwal, D.J. Eaglesham, J.B. Sapjeta, W.L. Brown, D.C. Jacobson, Y. Caudano, S.B. Christman and E.E. Chaban, 1997 Physics and Chemistry of Surfaces and Interfaces Conf., July 1997.
27. A. Aspar, et al., *Microelectronic Eng.* (36), 233 (1997).
28. O. Madelung, *Data in Science and Technology, Semiconductors,* (Springer-Verlag, 1991).
29. F. Ericson and J.A. Schweitz, *J. Appl. Phys.* 68, 5840 (1990).
30. M. Bruel, et al., *Jpn. J. Appl. Phys.* 36, 1636 (1997).
31. T.L. Anderson, *Fracture Mechanics, Fundamentals and Applications*, 2nd Ed., (Boca Raton, FL: CRC Press, 1995).
32. D. Broek, *Elementary Engineering Fracture Mechanism*, 4th Rev. Ed., (Martinus Nijhoff Publishers, 1987).
33. Y. B. Xin, et al. ACTA MATERIALIA, 44 (3), 845 (1996).
34. ABAQUS Finite Element Method, version 5.5 (1995).